LAWRENCE
LIVERMORE
NATIONAL
LABORATORY

LLNL-PROC-404677

Pillar Structured Thermal Neutron Detector

R.J. Nikolic, A.M. Conway, C.E. Reinhardt, R.T. Graff, T.F. Wang, N. Deo, C.L. Cheung

June 16, 2008

International Conference on Solid-State and Integrated-Circuit Technology
Beijing, China
October 20, 2008 through October 23, 2008

Disclaimer

Pillar Structured Thermal Neutron Detector

Rebecca J. Nikolic[1*], Adam M. Conway[1], Catherine E. Reinhardt[1], Robert T. Graff[1], Tzu-Fang Wang[1], Nirmalendu Deo[2], Chin Li Cheung[2]
[1] Lawrence Livermore National Laboratory, Livermore, CA 94550, USA
[2] University of Nebraska - Lincoln, Lincoln NE 68588, USA
*Email: nikolic1@llnl.gov

Abstract

This work describes an innovative solid state device structure that leverages advanced semiconductor fabrication technology to produce an efficient device for thermal neutron detection which we have coined the "Pillar Detector". State-of-the-art thermal neutron detectors have shortcomings in simultaneously achieving high efficiency, low operating voltage while maintaining adequate fieldability performance. By using a three dimensional silicon PIN diode pillar array filled with isotopic ^{10}boron (^{10}B), a high efficiency device is theoretically possible. Here we review the design considerations for going from a 2-D to 3-D device and discuss the materials trade-offs. The relationship between the geometrical features and efficiency within our 3-D device is investigated by Monte Carlo radiation transport method coupled with finite element drift-diffusion carrier transport simulations. To benchmark our simulations and validate the predicted efficiency scaling, experimental results of a prototype device are illustrated. The fabricated pillar structures reported in this work are composed of 2 μm diameter silicon pillars with a 2 μm spacing and pillar height of 12 μm. The pillar detector with a 12 μm height achieved a thermal neutron detection efficiency of 7.3% at a reverse bias of - 2 V.

1. Introduction

Thermal neutron detection is routinely carried out by utilizing ^{3}helium (^{3}He) tubes. Conventional ^{3}He tube neutron detectors can achieve very high thermal neutron detection efficiency. However, the use of these proportional counter type devices is encumbered by the required high operation voltage (1000 V), sensitivity to microphonics, large device footprint, and high tube pressure, all of which result in significant complications for routine deployment and air transport. These operating conditions make ^{3}He tubes difficult to use in the field. To overcome these problems, several solid state thermal neutron detector concepts have been recently developed [1]-[6].

Moving from a gas-based medium to a solid-state medium can dramatically reduce the size of the device because of the increase in the density of the neutron converter material. One approach for solid state thermal neutron detection is to coat the thermal neutron converter material on the top of a semiconductor material [4],[7], (see Figure 1a). Here, the neutron converter material is ^{10}B, which has a very high thermal neutron cross section of 3837 barns. When the thermal neutrons interact with ^{10}B, the energetic charged particles produced (alpha and $^{7}Li^{+}$) can then create electron-hole pairs within the semiconductor. Experience has revealed that single layers of this structure are limited to efficiencies of ~ 4% [4] because the range of the energetically favorable alpha particle is 3.6 μm in ^{10}B. In addition, stress in the ^{10}B film can further limit the thickness lower than that prescribed by range considerations alone. At the same time, a ^{10}B film thickness of approximately 54 μm (3 mean free paths) is needed to absorb the majority of the incoming thermal neutron flux, leading to conflicting design requirements for this device geometry.

The contradiction in scale lengths (3.6 μm versus 54 μm) is the hurdle to be overcome for producing high efficiency thermal neutron detectors using ^{10}B as the converter material. This conundrum can be resolved with our three dimensional "Pillar Detector" device. Even though ^{10}B is recognized as being an ideal neutron conversion material, progress has been limited due to the lack of available material processes. To date, the ability to fill high aspect ratio structures with ^{10}B remains a challenge. Fabrication of ^{10}B loaded semiconductors has been reported using evaporation and powder filling [5]. We have developed an approach utilizing chemical vapor deposition (CVD) with decaborane as the precursor to coat high aspect ratio structures with a conformal coverage [9].

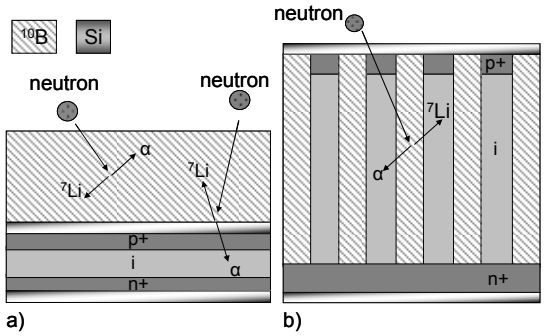

Figure 1. (a) 2-D solid state and (b) 3-D "Pillar Detector," with equal pillar diameter and spacing, arranged in a square matrix.

2. Pillar Detector Design

The contradiction in scale lengths (3.6 μm vs. 54 μm) has been resolved with our 3-D Pillar Detector [3],[6], as shown in Figure 1b. To achieve high efficiency, the design optimization simultaneously demands building up thicker regions of the converter material while capturing the energy from the energetic ions. The geometrical design considerations, material selection and resulting efficiency simulations are discussed below.

2.1 Neutron Conversion Material Selection

Candidate solid-state materials for use in thermal neutron detection are shown in Table 1, where the mean free path (mfp) is calculated by the inverse product of N (the nuclei per volume) and σ (the microscopic cross section). This can be illustrated by evaluating the probability of neutron interaction as a function of thickness t, η_{int} = 1-exp(-t/mfp). One approach led by a group of researchers at the University of Nebraska uses semiconducting ^{10}boron carbide [1]. In contrast to a "bulk" approach, Kansas State University researchers utilize a 3-D structure referred as silicon "perforation" technology with ^{6}LiF as the conversion material [2]. However, from Figure 2, it is evident that the highest probability amongst the candidate materials is the use of pure ^{10}B and $^{10}B_5C$. This can yield a thinner device for a given probability of interaction. Thinner device will correspondingly result in lower operation voltage and faster timing response.

Table 1. Comparison of neutron converter materials.

Material	Mean Free path (μm)
Natural Boron [8]	92
^{10}Boron [8]	18
Natural Boron Carbide (B_5C)[8]	113
^{10}Boron Carbide, ($^{10}B_5C$) [8]	21
^{6}Lithium Fluoride [10]	174

2.3 Pillar Spacing

The energy lost by the reaction by-products in the ^{10}B portion and deposited in the Si portion of the detector was tracked for each event using an energy dependent change in energy per unit distance (dE/dx). To calculate dE/dx for alpha and ^{7}Li in both the ^{10}B and Si portions of the detector, the Monte Carlo program Stopping Range of Ions in Matter (SRIM) was used. Lateral and longitudinal straggling was neglected in the simulation. Table 2 shows the average range of reaction by products in ^{10}B and Si for the both the ground state and 1st excited state. The neutron-^{10}B reaction is as follows:

1st excited state: $^{10}B + n \rightarrow \alpha + {}^{7}Li + \gamma$

Ground state: $^{10}B + n \rightarrow \alpha + {}^{7}Li$

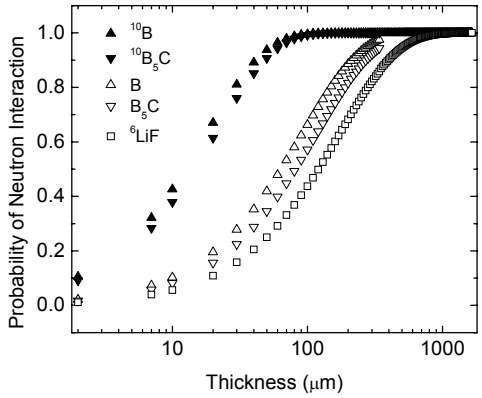

Figure 2. Calculation of thermal neutron interaction probability in ^{10}B and ^{6}LiF.

where the ground state has a probability of occurring 6% of the time and the first excited state 94% of the time. Both the ground state and the first excited state were simulated. The 0.48 MeV gamma generated by the first excited state is assumed to escape from the device.

Table 2. Range of ions in ^{10}B and Si.

	1st Excited State		Ground State	
Ion	Alpha	Li	Alpha	Li
Energy (MeV)	0.84	1.47	1.02	1.78
Distance in ^{10}B (μm)	1.85	3.6	2.0	4.4
Distance in Si (μm)	2.4	5.2	2.8	6.4

2.4 Efficiency Roadmap

The efficiency of the device is more complicated than range and mean free path considerations alone [11]. The thermalization process the neutrons undergo before striking the detector results in a random orientation of incident neutrons. The detection efficiency for a solid-state neutron detector is given by:

$$\eta_{tot} = \eta_{int} \cdot \eta_{conv} \cdot \eta_{semi} \cdot \eta_{rec} \qquad (1)$$

where η_{int} is the probability of neutron interaction with ^{10}B, η_{conv} is probability that energetic ions reach semiconductor detector, η_{semi} is the probability that energetic ions deposit enough energy in semiconductor to be detected, and η_{rec} is the efficiency reduction factor due to charge carrier recombination. The simulated total efficiency including all four efficiency components for several detector heights and geometries is shown in Figure 3. The efficiency scales with pillar height as a larger percentage of incident neutrons react with the ^{10}B. Also the efficiency scales inversely with diameter and spacing. For smaller pillar spacing, less energy is lost by the reaction by products before hitting the Si pillars.

For 1 μm diameter, 1 μm spacing and 100 μm height pillars an efficiency of 75% is predicted for a discriminator setting of 100 keV [11].

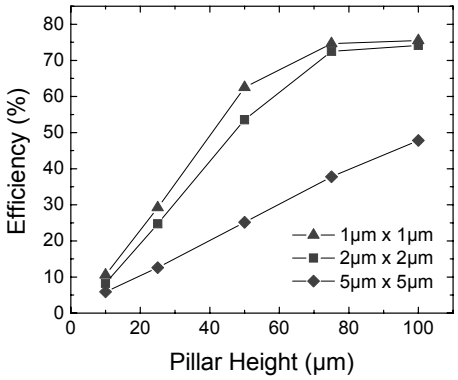

Figure 3. Pillar structured thermal neutron detector efficiency roadmap.

3. Fabrication

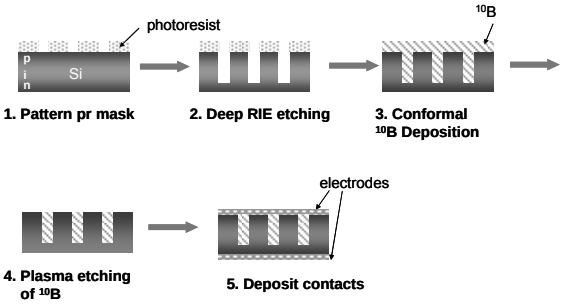

Figure 4. Multi-step fabrication process.

The fabrication process begins by epitaxially growing p+ and i layers on an n+ silicon substrate by using an ASM Epsilon CVD. The pillar diameter and spacing is then defined lithographically. Plasma etching is used to create high aspect ratio structures utilizing an SF_6 Bosch approach, followed by conformal coating of ^{10}B on the pillar array. The ability to deposit conformal and uniform coating of ^{10}B is one of the key steps to the success of the detector. Since the energetic ions are generated in the ^{10}B, any gap between the semiconductor and the boron layer will decrease the detector sensitivity. Using a thermal chemical vapor deposition (CVD) system with ^{10}B enriched decaborane as the precursor high fill factor ^{10}B filling has been achieved [9]. Next, the "etch-back" is carried out using a Plasmaquest electron cyclotron resonance etching (ECR) system with a tri-source gas mixture to expose the p+ layer for contact formation. Lastly, aluminum is sputtered onto the structures to fabricate the electrodes [6].

4. Characterization

Current versus voltage measurements were performed on a detector with 2 μm diameter pillars with 2 μm spacing and 12 μm pillar height (Figure 5) [6]. Low reverse biased current density of 1.8×10^{-4} A/cm^2 was measured at -1 V. Low leakage current is essential for high sensitivity to neutron events because this will set the noise floor for the device. The leakage current is comprised of bulk and surface components. The reverse biased current density of an unetched planar diode structure is on the order of 10^{-7} A/cm^2, implying that the increase in leakage current is due to surface recombination. Further reduction of the leakage current can be achieved by passivating the large surface area side walls. Low voltage is also important for low power devices. The intrinsic region has a free carrier concentration of 10^{13} cm^{-3} which requires -0.8 V for depletion. The neutron response of this detector was measured using a fission neutron source moderated by polyethylene blocks to yield thermal neutrons. A thermal neutron detection efficiency of 7.3 % was achieved at -2 V (Figure 6).

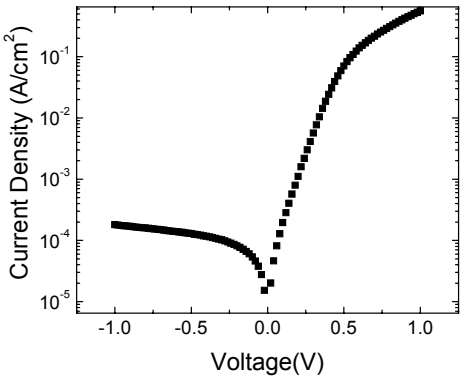

Figure 5. Current-voltage measurement of Pillar Detector, (2 μm diameter, 2 μm spacing, 12 μm height).

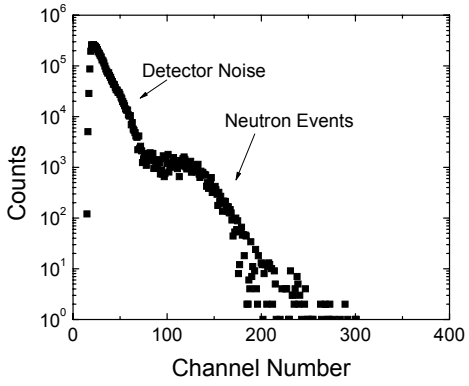

Figure 6. The energy response of Pillar Detector. A ^{252}Cf neutron source moderated via polyethylene was used in the measurement with a reverse bias of -2 V, (2 μm diameter, 2 μm spacing, 12 μm height).

5. Pillar Detector Scaling

The simulated efficiency data from Figure 3 is plotted against our measured results (2 μm diameter pillar with a 2 μm spacing, 12 μm height) as shown in Figure 7. The required aspect ratio for high efficiency will be on the order of 25:1, for a 50 μm tall pillar, which is well within the state-of-the art for plasma etching techniques [12]. Figure 7 shows our status of pillar etch and fill technology of 25:1 aspect ratio.

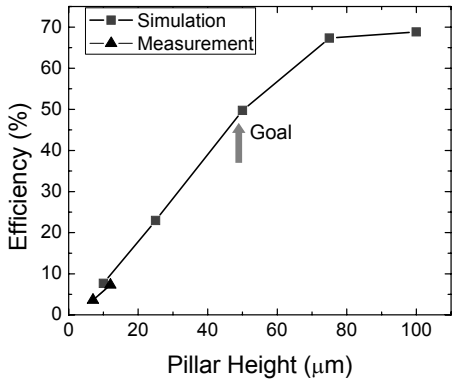

Figure 7. Comparison of our simulated efficiency (discriminator at 300 keV) curve (2 μm diameter pillar, 2 μm spacing) with our experimentally derived measurements, showing the device can scale to high efficiency.

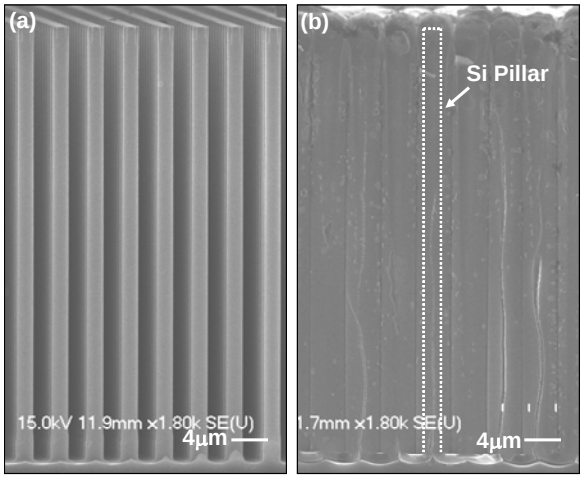

Figure 8. SEM photos of 50 μm tall Si pillars with a 2 μm diameter and 2 μm spacing (a) before ^{10}B CVD and (b) after ^{10}B CVD with ~ 98-99 % fill factor.

6. Summary

In summary, we have developed an innovative device that can take advantage of the high thermal neutron cross section of ^{10}B by accommodating a large fraction of this material while simultaneously addressing the conflicting length scales of neutron absorption and the resulting by-product ranges. The first radiation results of our proof-of-principle device show 7.3% efficiency with an aspect ratio of 6:1. This is the best result for a thermal neutron detector based on ^{10}B without a stacking configuration. It is a major step towards scaling to a depth of 50+ μm for high efficiency thermal neutron detection.

Acknowledgments

This work performed under the auspices of the U.S. Department of Energy by Lawrence Livermore National Laboratory under Contract DE-AC52-07NA27344, LLNL-PROC-404677.

References

1. K. Osberg, N. Schemm, S. Balkir, J.I. Brand, M.S. Hallbeck, P.A. Dowben, and M.W. Hoffman, IEEE Sensors Journal, vol. 6, no. 6, pp.1531-1538, 2006.
2. J.K. Shultis and D.S. McGregor, IEEE Transactions on Nuclear Science, vol.53, no.3, pp. 1659-1665, 2006.
3. R.J. Nikolic, C.L. Cheung, C.E. Reinhardt, and T.F. Wang, SPIE-Int. Soc. Opt. Eng. Proceedings of the SPIE, Photonics West, vol. 6013, no.1, pp. 36-44, Boston, MA, 2005.
4. D.S. McGregor, R.T. Klann, H.K. Gersch, and Y.H. Yang, Nuclear Instruments and Methods in Physics Research A, vol. 466, pp. 126-141, 2001.
5. D.S. McGregor, R.T. Klann, H.K. Gersch, E. Ariesanti, J.D. Sanders, and B. Van Der Elzen, IEEE Transactions on Nuclear Science, vol. 49, pp. 1999-2004, 2002.
6. R.J. Nikolic, A.M. Conway, T. Graff, C.E. Reinhardt, T.F. Wang, N. Deo, and C.L. Cheung, 2007 IEEE Nuclear Science Symposium, Conference record N24-342, Honolulu, Hawaii, pp. 1577-1580, Oct. 2007.
7. A. Rose, Nuclear Instruments and Methods, vol. 52, pp. 166-170, 1967.
8. D.S. McGregor, M.D. Hammig, Y.-H. Yang, H.K. Gersch, and R.T. Klann, Nuclear Instruments and Methods in Physics Research A, vol. 500, pp. 272-308, 2003.
9. N. Deo, J.R. Brewer, C.E. Reinhardt, R.J. Nikolic and C.L. Cheung, Journal of Vacuum Science and Technology B, July/Aug, 2008.
10. D.R. Lide, CRC Handbook of Chemistry and Physics, Boca Raton, FL, CRC Press, 2002.
11. A.M. Conway, T.F. Wang, N. Deo, and C.L. Cheung, R.J. Nikolic, special conference issue of the IEEE Transactions on Nuclear Science (TNS), in preparation.
12. F. Ayazi, and K. Najafi, Sensors and Actuators, vol. 87, pp. 46-51, 2000.